ZEUS-prel-06-021

Submitted to the
XXIII International Conference on High Energy Physics
July 26-August 2, Moscow, Russia

Abstract: **Session: QCD hard interactions**

Measurement of charm production in deep inelastic scattering at HERA II

Abstract

Inclusive production of $D^*(2010)$ mesons in deep inelastic scattering has been measured with the ZEUS detector at HERA II using the data taken during the 2003-5 running period. Differential D^* cross sections are compared to next-to-leading-order QCD predictions.

1 Introduction

Charm quarks are copiously produced in deep inelastic scattering (DIS) at HERA. At sufficiently high photon virtuality, Q^2, the production of charm quarks constitutes up to 30% of the total cross section [1,2]. Previous measurements of D^* cross sections [1,2,3,4,5] indicate that the production of charm quarks in DIS in the range of $1 < Q^2 < 1000\,\mathrm{GeV}^2$ is consistent with calculations in Quantum Chromodynamics (QCD) in which charm is produced via boson-gluon-fusion (BGF). This implies that the charm cross section is directly sensitive to the gluon density in the proton.

In this paper, measurements of the D^* cross section are presented which have comparable precision to the ZEUS HERA I measurement [5] and which extend the kinematic region to larger pseudorapidity, $\eta(D^*)$. Single differential cross sections have been measured as a function of Q^2, the transverse momentum, $p_T(D^*)$, and $\eta(D^*)$ of the D^* meson. The cross sections are compared to a next-to-leading-order (NLO) QCD calculation using the ZEUS NLO QCD fit, in which the parton densities in the proton have been parameterised by fitting inclusive DIS measurements from ZEUS and fixed-target experiments.

2 Experimental set-up

A detailed description of the ZEUS detector can be found elsewhere [6]. The main components used in this analysis were the compensating uranium-scintillator calorimeter, the central tracking detector and the micro-vertex detector.

The high-resolution uranium–scintillator calorimeter (CAL) [7] consists of three parts: the forward (FCAL), the barrel (BCAL), and the rear (RCAL) calorimeters. The CAL is the major component used for the reconstruction of the DIS kinematic variables.

Charged particles are tracked in the central tracking detector (CTD) [8], which operates in a magnetic field of 1.43 T provided by a thin superconducting coil.

In 2001 a silicon micro-vertex detector (MVD) [9] was installed inside the CTD. The MVD is organised into a barrel with 3 cylindrical layers and a forward section with four planar layers perpendicular to the HERA beam direction. A combination of CTD and MVD information was used to reconstruct D^* mesons.

3 Event sample

An inclusive selection of neutral current DIS events which was directly comparable to the previous measurement [5] was made. Events were required to have a reconstructed vertex within 30 cm of the nominal interaction point in Z. The quantity

$$\delta = E - p_z = \sum_i E_i(1 - \cos\theta_i),$$

was calculated using the energies, E_i, and polar angles θ_i of all calorimeter cells above noise threshold. For events where no energy escapes through the rear beam hole, δ should be equal to $2E_e = 55\,\text{GeV}$. Events are required to satisfy $40 < \delta < 60\,\text{GeV}$, to eliminate photoproduction events or DIS events with high-energy initial-state radiation, in which the scattered electron, or the radiated photon, respectively escape through the rear beam hole.

The variables Q^2 and y were reconstructed in terms of the energy E'_e and angle θ_e of the scattered electron:

$$\begin{aligned} Q_e^2 &= 2E'_e E_e(1 + \cos\theta_e) \\ y_e &= 1 - \frac{E'_e}{2E_e}(1 - \cos\theta_e), \end{aligned}$$

where E_e is the electron beam energy. The variable y was also reconstructed from the hadronic system using the Jaquet-Blondel method,

$$y_{\text{JB}} = \frac{1}{2E_e} \sum_{i \in \text{hfs}} E_i(1 - \cos\theta_i),$$

where the sum runs over only those calorimeter cells assigned to the hadronic final state.

The cuts $5 < Q_e^2 < 1000\,\text{GeV}^2$, $y_{\text{JB}} > 0.02$, and $y_e < 0.7$ define the kinematic region of the measurement.

4 Selection of D^* candidates

The selection of D^* mesons also followed the strategy used in the previous publication [5]. The D^* mesons were identified using the decay channel $D^{*+} \to D^0\pi_s$ with the subsequent decay $D^0 \to K^-\pi^+$ and the corresponding antiparticle decay, where π_s^+ refers to a low momentum ("slow") pion accompanying the D^0.

Primary-vertex tracks which had transverse momentum $p_T > 0.12\,\text{GeV}$ and for which the pseudorapidity, η, satisfied $|\eta| < 1.75$ were selected. These restrictions ensured that the track acceptance and momentum resolution were high. Tracks with opposite charges and $p_T > 0.4\,\text{GeV}$ were combined in pairs to form D^0 candidates. The tracks were alternately assigned the kaon and pion masses and the invariant mass of the pair, $M_{K\pi}$, was calculated.

Each additional track, with charge opposite to that of the kaon track, was assigned the pion mass and combined with the D^0-meson candidate to form a D^* candidate.

The signal regions for the reconstructed masses, $M(D^0)$ and $\Delta M = M_{K\pi\pi_s} - M_{K\pi}$, were $1.80 < M(D^0) < 1.92\,\text{GeV}$ and $0.143 < \Delta M < 0.148\,\text{GeV}$, respectively. To determine the combinatorial background, wrong-charge D^* candidates in which both tracks forming the D^0 candidates have the same charge and the third track has the opposite charge, were used.

The kinematic region for D^* candidates was $1.5 < p_T(D^*) < 15$ GeV and $|\eta(D^*)| < 1.5$. Figure 1 shows the ΔM distribution for the D^* candidates and also for the wrong-charge combinations. The fit to the distribution, shown in in the figure, has the form:

$$F = p_1 \exp\left(-\frac{1}{2}x^{1+\frac{1}{1+0.5x}}\right) + p_4(\Delta M - m_\pi)^{p_5},$$

where $x = |(\Delta M - p_2)/p_3|$, the p_i are free parameters, and m_π is the pion mass.

The number of reconstructed D^*'s was determined by subtracting the wrong-charge background from the correct-charge candidates in the region $0.143 < \Delta M < 0.148\,\text{GeV}$. The normalisation of the wrong-charge background sample was determined as the ratio of events with correct-charge combinations to wrong-charge combinations in the region $0.150 < \Delta M < 0.165\,\text{GeV}$. The number of D^* mesons selected in the kinematic region $5 < Q^2 < 1000$ GeV^2, $0.02 < y < 0.7$, $1.5 < p_T(D^*) < 15$ GeV, and $|\eta(D^*)| < 1.5$, was 5898 ± 148 (see Fig. 1).

The differential D^* production cross section in observable Y was determined using

$$\frac{d\sigma}{dY} = \frac{N}{A \cdot \mathcal{L} \cdot B \cdot \Delta Y},$$

where N is the number of reconstructed D^* mesons in a bin of width ΔY. The acceptance, A, takes into account migrations and efficiencies for that bin, and $\mathcal{L}$ is the integrated luminosity. For the branching ratio, $B = BR(D^{*+} \rightarrow D^0\pi^+) \times BR(D^0 \rightarrow K^-\pi^+)$, the value $(2.57 \pm 0.06)\%$ [10] was used.

5 Monte Carlo samples

The acceptances were calculated using RAPGAP 2.08 [11] and HERWIG 6.301 [12] Monte Carlo (MC) models. The generated events were then passed through a full GEANT 3.13-based detector and trigger simulation and were analyzed with the same programs as used for the data.

Figure 2 shows the distributions of the DIS variables for D^* events (after background subtraction) for data compared to the detector-level RAPGAP predictions. The RAPGAP predictions are in reasonable agreement with the data distributions for both the scattered-electron and hadronic variables. The HERWIG MC gives a similarly reasonable representation of the data (not shown) and is used to estimate the systematic uncertainty, arising from the model in the correction procedure.

6 Experimental and theoretical uncertainties

6.1 Experimental uncertainties

Cross checks of the result were made by varying the selection cuts as described in previous publications [5,13]. In addition it was verified that extracting the number of reconstructed D^* mesons in each bin using the fit described in Section 4 gave results which were consistent with the background subtraction based on the wrong-charge candidates.

6.2 Theoretical uncertainties

The program HVQDIS [14] was used to calculate NLO QCD predictions for D^* production. The following systematic uncertainties in the calculation were considered.

- The gluon PDF in the proton was varied from the default (the ZEUS NLO QCD fit). Cross sections were recalculated using the CTEQ5F3 [15] and GRV98-HO [16] parameterisations. The charm masses appropriate to each parameterisation were used in HVQDIS: 1.3 GeV for CTEQ5F3 and 1.4 GeV for GRV98-HO. The change in the cross section was $+2.0\%$ using CTEQ5F3 and -16% using GRV98-HO.
- The mass of the charm quark was varied. The charm mass was changed consistently in the PDF fit and in HVQDIS from the central value of 1.35 GeV by ∓ 0.15 GeV resulting in a $\left(^{+9.7}_{-9.1}\%\right)$ change in the cross section. The largest effect was at low $p_T(D^*)$.
- The renormalisation and factorisation scale, μ was modified from the nominal value of $\sqrt{Q^2 + 4m_c^2}$ to $2\sqrt{Q^2 + 4m_c^2}$ and $\max(2m_c, \sqrt{Q^2/4 + m_c^2})$ [14]. These variations changed the cross sections typically by $\left(^{+4}_{-1}\%\right)$.

7 Results and conclusions

In Fig. 3, the differential cross section in Q^2 is compared to the previous HERA I result. Good agreement is seen for the entire Q^2 range over which the differential cross section falls by about four orders of magnitude. In Fig. 4, the cross-section $d\sigma/dp_T(D^*)$ is seen to fall by two orders of magnitude with increasing $p_T(D^*)$. Fig. 5 shows the cross-section $d\sigma/d\eta(D^*)$. The data are compared with the NLO QCD calculation implemented in the HVQDIS program. The cross sections as a function of Q^2 , $p_T(D^*)$, and $\eta(D^*)$ are reasonably well described by the NLO calculation.

The extension to the forward $\eta(D^*)$ region will yield smaller extrapolation factors when extracting the proton structure function $F_2^{c\bar{c}}$. The HERA I and HERA II results will be combined in the future, leading to a higher precision estimation of $F_2^{c\bar{c}}$.

References

[1] ZEUS Coll., J. Breitweg et al., Eur. Phys. J. **C 12**, 35 (2000).

[2] H1 Coll., C. Adloff et al., Phys. Lett. **B 528**, 199 (2002).

[3] ZEUS Coll., J. Breitweg et al., Phys. Lett. **B 407**, 402 (1997).

[4] H1 Coll., C. Adloff et al., Nucl. Phys. **B 545**, 21 (1999).

[5] ZEUS Coll., S. Chekanov et al., Phys. Rev. **D 69**, 012004 (2004).

[6] ZEUS Coll., U. Holm (ed.), *The ZEUS Detector*. Status Report (unpublished), DESY (1993), available on `http://www-zeus.desy.de/bluebook/bluebook.html`.

[7] M. Derrick et al., Nucl. Inst. Meth. **A 309**, 77 (1991);
A. Andresen et al., Nucl. Inst. Meth. **A 309**, 101 (1991);
A. Caldwell et al., Nucl. Inst. Meth. **A 321**, 356 (1992);
A. Bernstein et al., Nucl. Inst. Meth. **A 336**, 23 (1993).

[8] N. Harnew et al., Nucl. Inst. Meth. **A 279**, 290 (1989);
B. Foster et al., Nucl. Phys. Proc. Suppl. **B 32**, 181 (1993);
B. Foster et al., Nucl. Inst. Meth. **A 338**, 254 (1994).

[9] E.N. Koffeman et al., Nucl. Inst. Meth. **A 453**, 89 (2000);
D. Dannheim et al., Nucl. Inst. Meth. **A 505**, 663 (2003).

[10] S. Eidelman et al., Phys. Lett. **B592**, 1 (2004).

[11] H. Jung, Comp. Phys. Commun. **86**, 147 (1995).

[12] G. Corcella et al., HERWIG 6.3 release note (2001).

[13] ZEUS Coll., S. Chekanov et al., Eur. Phys. J. **C44**, 351 (2005).

[14] B. W. Harris and J. Smith, Phys. Rev. **D57**, 2806 (1998).

[15] CTEQ Coll. H.L.Lai et al., Eur. Phys. J. **C 12**, 375 (2000) .

[16] M. Glück, E. Reya and A. Vogt, Eur. Phys. J. **C 5**, 461 (1998).

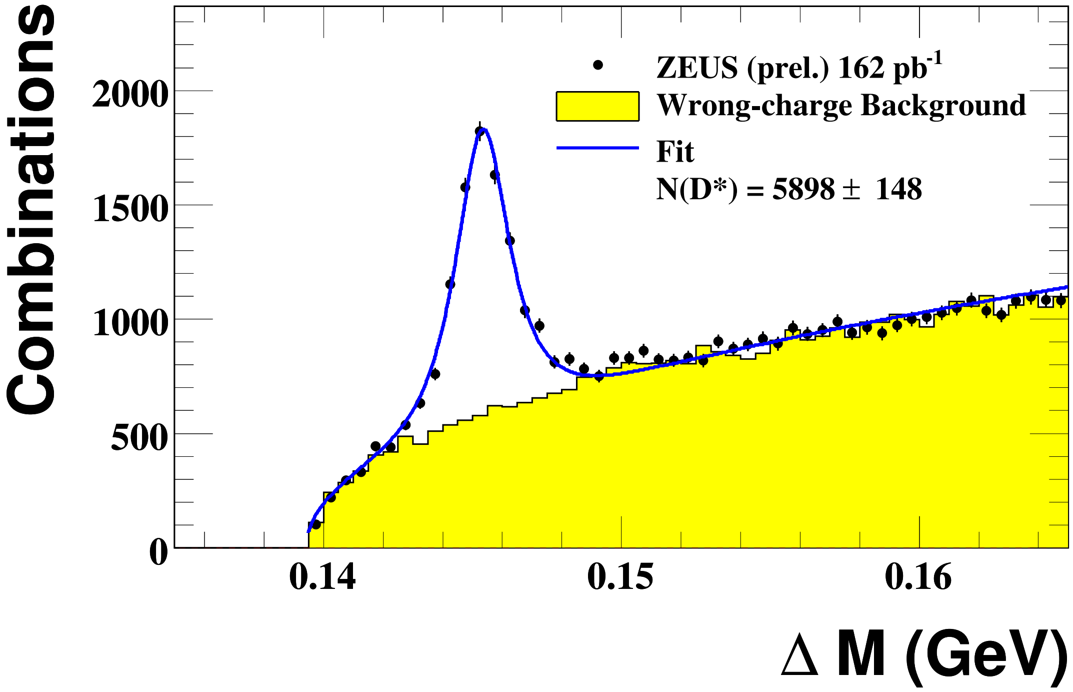

Figure 1: *The distribution of the mass difference, $\Delta M = M_{K\pi\pi_s} - M_{K\pi}$, for D^* candidates in $e^{\pm}p$ scattering (solid dots). The ΔM distribution from wrong-charge combinations, normalised in the region $0.150 < \Delta M < 0.165$ GeV, is shown as the shaded histogram. The solid line shows the result of the fit described in the text.*

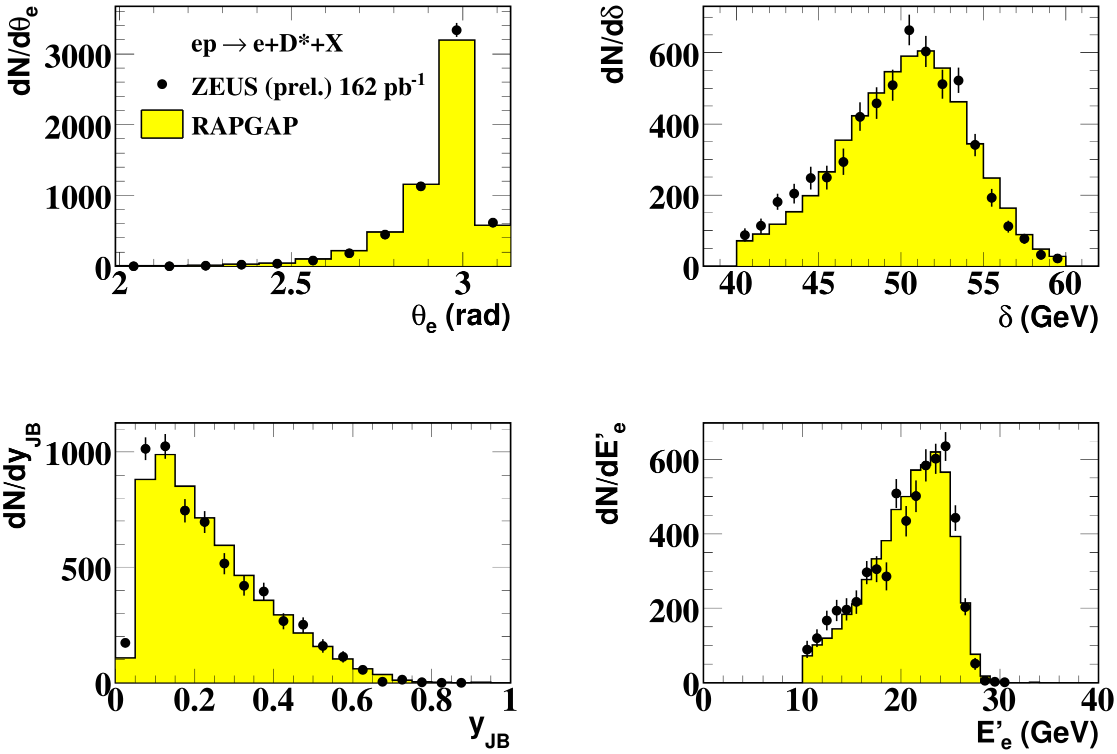

Figure 2: *Reconstructed DIS variables for events with D^* candidates (after background subtraction) for data (points) compared to detector-level RAPGAP predictions (shaded histograms).*

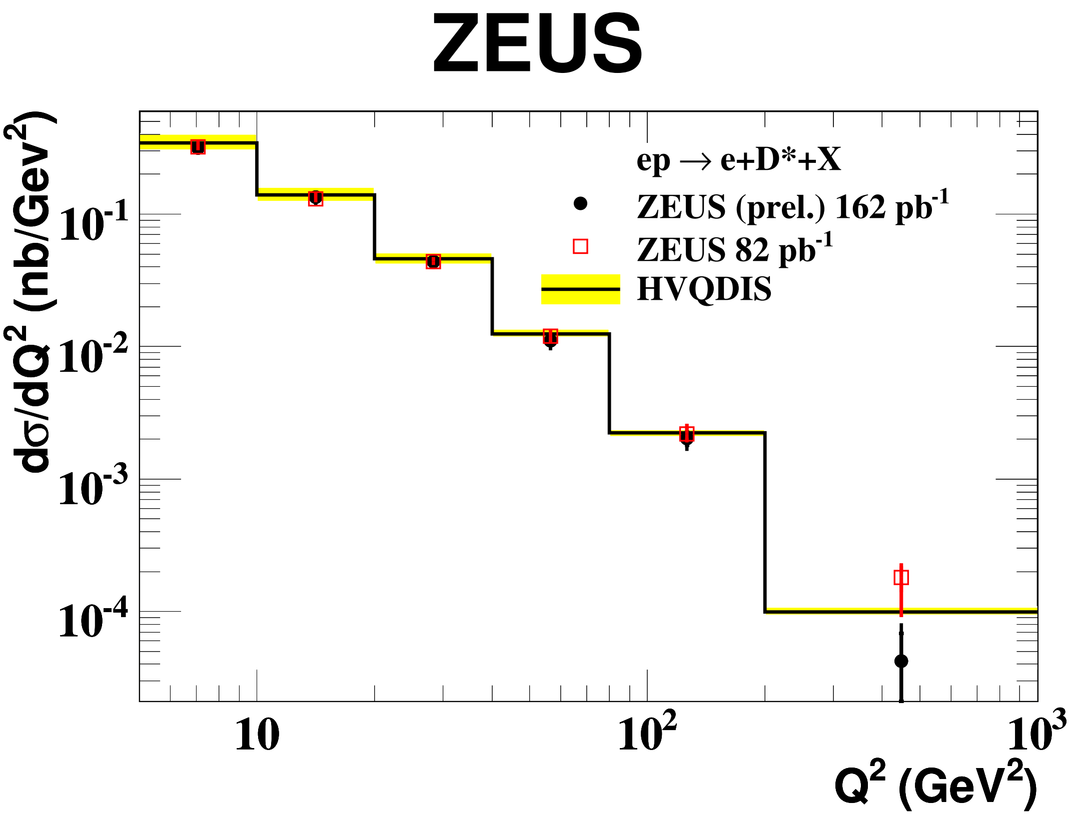

Figure 3: *Differential D^* cross section as a function of Q^2 compared to the NLO QCD calculation of HVQDIS. The HERA II data (solid points) are shown compared to the most recently published ZEUS measurement (open squares). The inner error bars indicate the statistical uncertainties and the outer bars show the statistical and systematic uncertainties added in quadrature. The solid line gives the predictions from the ZEUS NLO QCD fit for $m_c = 1.35\,GeV$ with the shaded band indicating the uncertainty in the prediction.*

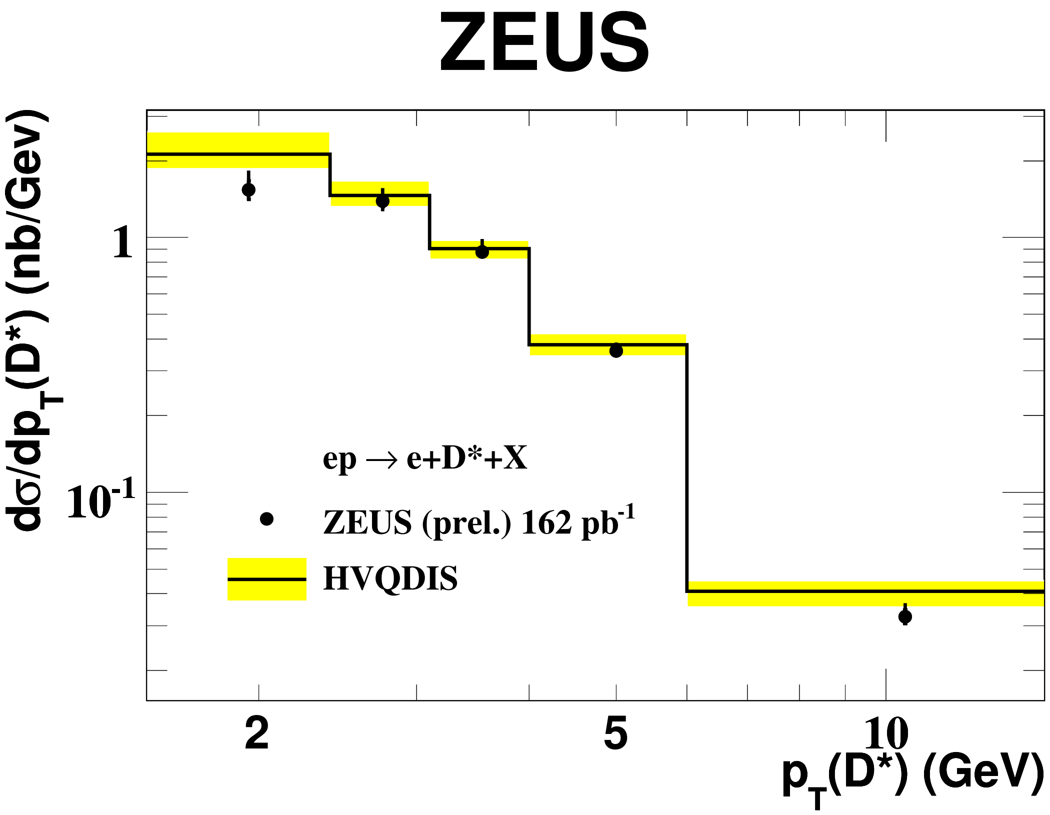

Figure 4: *Differential D^* cross section as a function of $p_T(D^*)$ compared to the NLO QCD calculation of HVQDIS. The solid points show the HERA II data with the inner error bars indicating statistical uncertainties and the outer bars showing statistical and systematic uncertainties added in quadrature. The solid line gives the predictions from the ZEUS NLO QCD fit for $m_c = 1.35\,GeV$ with the shaded band indicating the uncertainty in the prediction.*

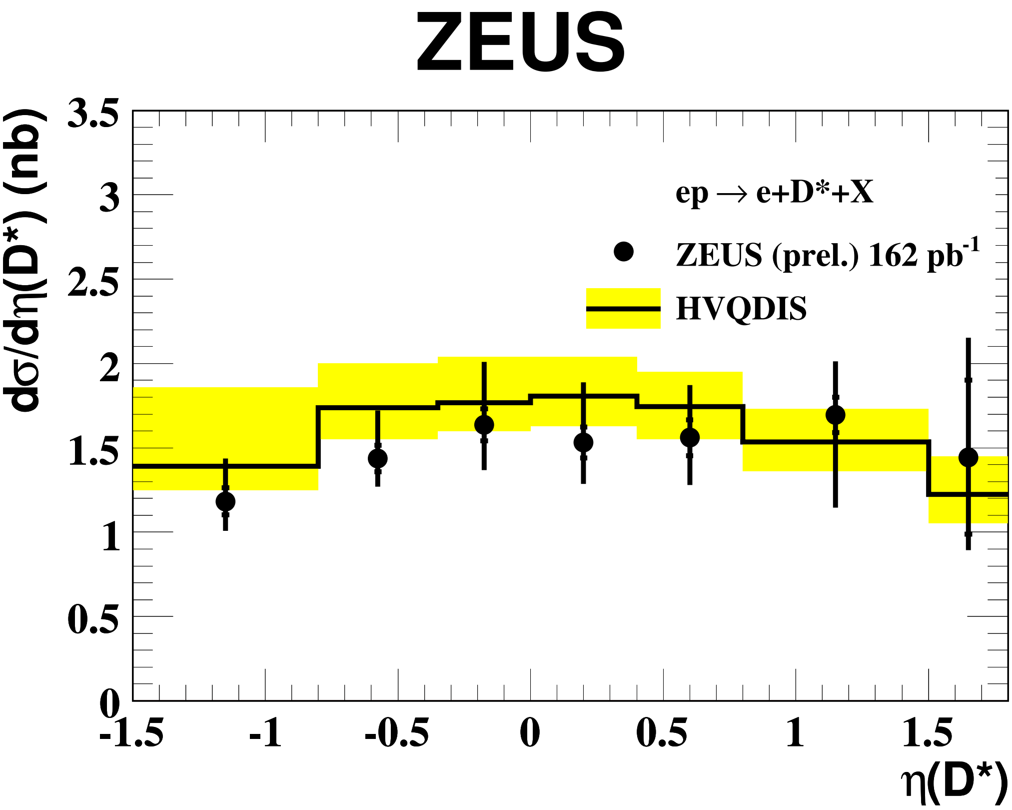

Figure 5: *Differential D^* cross section as a function of $\eta(D^*)$ compared to the NLO QCD calculation of HVQDIS. The solid points show the HERA II data with the inner error bars indicating the statistical uncertainties and the outer bars showing the statistical and systematic uncertainties added in quadrature. The solid line gives the predictions from the ZEUS NLO QCD fit for $m_c = 1.35\ GeV$ with the shaded band indicating the uncertainty in the prediction.*